The Astrophysical Journal, 615:934–946, 2004 November 10

REACTION RATE UNCERTAINTIES AND THE PRODUCTION OF ^{19}F IN ASYMPTOTIC GIANT BRANCH STARS

Maria Lugaro
Institute of Astronomy, University of Cambridge, Madingley Road, Cambridge CB3 0HA, UK; mal@ast.cam.ac.uk

Claudio Ugalde
The Joint Institute for Nuclear Astrophysics and Department of Physics, University of Notre Dame, 225 Nieuwland Science Hall, Notre Dame, IN 46556; ugalde.1@nd.edu

Amanda I. Karakas
Institute for Computational Astrophysics, Department of Astronomy and Physics, Saint Mary's University, Halifax, NS B3H 3C3, Canada; akarakas@ap.stmarys.ca

Joachim Görres and Michael Wiescher
The Joint Institute for Nuclear Astrophysics and Department of Physics, University of Notre Dame, 225 Nieuwland Science Hall, Notre Dame, IN 46556; wiescher.1@nd.edu, goerres.1@nd.edu

John C. Lattanzio
School of Mathematical Sciences, P.O. Box 28M, Monash University, Victoria 3800, Australia; j.lattanzio@sci.monash.edu.au

and

Robert C. Cannon
Institute of Adaptive and Neural Computation, Division of Informatics, 5 Forrest Hill, Edinburgh EH1 2QL, UK; robert.cannon@ed.ac.uk
Received 2003 November 15; accepted 2004 July 19

ABSTRACT

We present nucleosynthesis calculations and the resulting ^{19}F stellar yields for a large set of models with different masses and metallicity. During the asymptotic giant branch (AGB) phase, ^{19}F is produced as a consequence of nucleosynthesis occurring during the convective thermal pulses and also during the interpulse periods if protons from the envelope are partially mixed in the top layers of the He intershell (partial mixing zone). We find that the production of fluorine depends on the temperature of the convective pulses, the amount of primary ^{12}C mixed into the envelope by third dredge-up, and the extent of the partial mixing zone. Then we perform a detailed analysis of the reaction rates involved in the production of ^{19}F and the effects of their uncertainties. We find that the major uncertainties are associated with the ^{14}C$(\alpha, \gamma)^{18}$O and ^{19}F$(\alpha, p)^{22}$Ne reaction rates. For these two reactions we present new estimates of the rates and their uncertainties. In both cases the revised rates are lower than previous estimates. The effect of the inclusion of the partial mixing zone on the production of fluorine strongly depends on the very uncertain ^{14}C$(\alpha, \gamma)^{18}$O reaction rate. The importance of the partial mixing zone is reduced when using our estimate for this rate. Overall, rate uncertainties result in uncertainties in the fluorine production of about 50% in stellar models with mass $\simeq 3\ M_{\odot}$ and of about a factor of 7 in stellar models of mass $\simeq 5\ M_{\odot}$. This larger effect at high masses is due to the high uncertainties of the ^{19}F$(\alpha, p)^{22}$Ne reaction rate. Taking into account both the uncertainties related to the partial mixing zone and those related to nuclear reactions, the highest values of ^{19}F enhancements observed in AGB stars are not matched by the models. This is a problem that will have to be revised by providing a better understanding of the formation and nucleosynthesis in the partial mixing zone, as well as in relation to reducing the uncertainties of the ^{14}C$(\alpha, \gamma)^{18}$O reaction rate. At the same time, the possible effect of cool bottom processing at the base of the convective envelope should be included in the computation of AGB nucleosynthesis. This process could, in principle, help to match the highest ^{19}F abundances observed by decreasing the C/O ratio at the surface of the star, while leaving the ^{19}F abundance unchanged.

Subject headings: nuclear reactions, nucleosynthesis, abundances — stars: AGB and post-AGB — stars: carbon

1. INTRODUCTION

Spectroscopic observations show that in giant stars of type K, M, MS, S, SC, and C the fluorine abundance is enhanced by factors of 2–30 with respect to the solar abundance (Jorissen et al. 1992). These low-mass stars are the only astrophysical site observationally confirmed to produce fluorine. Hence, they are good candidates to account for the Galactic abundance of this element, even though recent observations of ^{19}F in the LMC and ω Cen, where the abundance ratio of F/O declines with the oxygen abundance, may support the hypothesis that most fluorine is produced instead by massive stars (Cunha et al. 2003; Renda et al. 2004). In any case, the fluorine abundances observed in giant stars are of considerable importance in constraining the properties of asymptotic giant branch (AGB) models. In AGB stars H and He shell burning with subsequent He pulse driven convection (thermal pulse) changes the abundance distribution between the H- and He-burning shells (He intershell). Partial He burning in the He intershell converts He into ^{12}C. After the occurrence of a thermal pulse, the convective envelope can penetrate the He intershell and dredge up material to the surface (third dredge-up [TDU]). The stellar atmosphere becomes progressively rich in carbon, thus explaining the observed sequence of carbon enrichment from M to S and C stars. These stars also show enhancements of elements produced by slow neutron captures (*s*-process) and are

believed to be the main site for the production of *s*-process nuclei with mass above $\simeq$90 (Gallino et al. 1998; Travaglio et al. 1999, 2001; Goriely & Mowlavi 2000).

The observed enhancements of fluorine in AGB stars indicate a positive correlation with the carbon enhancements. This can be explained if ^{19}F is also produced in the He intershell and then dredged up to the surface together with ^{12}C and *s*-process elements. Jorissen et al. (1992) proposed the following nucleosynthesis path for the production of ^{19}F in the He intershell of AGB stars. Neutrons produced via the ^{13}C(α, n)^{16}O reaction can be captured by ^{14}N, which is enriched from the preceding H-burning stage where the CNO cycle dominates. The reaction ^{14}N(n, p)^{14}C has a high cross section and produces free protons and ^{14}C, which is converted by α-capture to ^{18}O; alternatively, ^{18}O can also be produced by α-capture on ^{14}N with subsequent β-decay of ^{18}F. In core He burning, ^{18}O is converted by further α-capture to produce ^{22}Ne via the reaction ^{18}O(α, γ)^{22}Ne; however, in the He intershell ^{18}O and protons are present at the same time, triggering the alternative reaction path ^{18}O(p, α)^{15}N. Subsequent α-capture on ^{15}N eventually leads to the production of ^{19}F, via ^{15}N(α, γ)^{19}F. The ^{15}N(p, α)^{12}C reaction competes with the ^{18}O(p, α)^{15}N reaction and removes both protons and ^{15}N from the chain of production of ^{19}F. The abundance of ^{19}F is determined by the reaction rates associated with this rather complex production path and by the ^{19}F destruction reaction in the He intershell, ^{19}F(α, p)^{22}Ne.

In summary, the reactions that contribute to or affect the production of fluorine are ^{13}C(α, n)^{16}O, ^{14}N(n, p)^{14}C, ^{14}N(α, γ)^{18}F, ^{14}C(α, γ)^{18}O, ^{18}O(α, γ)^{22}Ne, ^{15}N(p, α)^{12}C, together with the alternative reaction chain ^{18}O(p, α)^{15}N(α, γ)^{19}F(α, p)^{22}Ne. The theoretical studies of Forestini et al. (1992) and Mowlavi et al. (1996) found that the above-described chain is activated in the convective pulse when neutrons are released by ^{13}C from the H-burning ashes. However, only the lowest observed abundances of ^{19}F could be explained. An extra amount of ^{13}C is required to produce the observed ^{19}F and also to match the observed enhancements of *s*-process elements. At the end of each TDU where the convective envelope expands into the stable radiative intershell zone, extra mixing processes could lead to the formation of a zone where protons and ^{12}C are partially mixed (partial mixing zone). This would lead to additional production of ^{13}C by the ^{12}C(p, γ) reaction in the top layers of the He intershell. Models including hydrodynamical overshoot (Herwig 2000), rotation (Langer et al. 1999), or the effect of gravity waves (Denissenkov & Tout 2003) have in fact produced a partial mixing zone resulting in the formation of a ^{13}C "pocket." Straniero et al. (1995) showed that the ^{13}C formed in the pocket is completely destroyed by the ^{13}C(α, n)^{16}O reaction before the onset of the next convective pulse. By means of a parametric representation of the partial mixing zone, Gallino et al. (1998) and Goriely & Mowlavi (2000) showed that this model can explain the observed properties of the *s*-process in AGB stars. In the ^{13}C pocket ^{15}N is produced at conditions where the value of the proton-to-^{12}C ratio is close to unity (see also Mowlavi et al. 1998). This ^{15}N is converted into ^{19}F when the pocket is ingested in the following convective pulse. Goriely & Mowlavi (2000) analyzed the effect of the presence of the partial mixing zone on the nucleosynthesis of fluorine. These authors concluded that also by taking into account the nucleosynthesis in the partial mixing zone only the less fluorine-enriched stars could be explained. The possible effect on the nucleosynthesis in the partial mixing zone due to stellar rotation also did not seem to improve the match with observations (Herwig et al. 2003).

The aims of this paper are to update the study of the production of ^{19}F in AGB stars and to explore the impact of the uncertainties of nuclear reaction rates on the abundance of fluorine produced in the framework of the current AGB star models. First, we introduce the production of ^{19}F in AGB models of a large range of masses and metallicities. We calculate the stellar structure and then follow the nucleosynthesis by making use of a postprocessing code. Our computations represent an improvement with respect to previous computations for several reasons. First, we find the TDU to occur self-consistently after a certain number of thermal pulses; hence, we do not parameterize this process as done in all the previous studies. If it is true that the amount of TDU is still uncertain (see, e.g., Frost & Lattanzio 1996; Mowlavi 1999) and hence can be parameterized, our approach is more consistent in the fact that we not only deal with TDU as a way of mixing fluorine to the stellar surface but also take into account the feedback effect of TDU on the nucleosynthesis of ^{19}F in the He intershell. As we show, this feedback has a large impact on the production of ^{19}F. Second, our postprocessing code follows the nucleosynthesis throughout all the different thermal pulses previously computed by the evolutionary code. This was done by Mowlavi et al. (1996) for three stellar models with a limited number of pulses, but without including a partial mixing zone. Goriely & Mowlavi (2000) included a partial mixing zone in their calculations but only followed the nucleosynthesis "during one representative interpulse and pulse phase," hence missing the possible effects due to variations of the thermodynamic features of each thermal pulse. Finally, our postprocessing code computes abundances of nuclei up to iron, solving simultaneously the changes due to nuclear reactions and those due to mixing, when convection is present. This allows us, for example, to properly model the nucleosynthesis that occurs at the delicate moment when the H-burning ashes are progressively ingested in the convective pulse and the ^{13}C present in the ashes burns via the (α, n) reaction while the ingestion is occurring.

We discuss and compare results from a large set of stellar models, analyze in detail the impact of the introduction of the partial mixing zone and of the reaction rate uncertainties on the 3 $M_\odot$ $Z = 0.02$ model, and then present upper and lower limits for the production of fluorine in several selected models. On top of the comparison with spectroscopic observations of AGB stars, our results are of relevance when studying the Galactic chemical evolution of fluorine, as done recently by Renda et al. (2004). The evolutionary and nucleosynthesis codes are presented in § 2. The production of fluorine in a large range of stellar models is discussed in § 3. The effect of introducing a partial mixing zone is discussed in § 3.1. The nuclear reactions contributing to the production of ^{19}F are discussed in § 4, together with the effect of their uncertainties on the production of ^{19}F. In § 5 we present a final discussion and possible directions for future work.

2. EVOLUTIONARY AND NUCLEOSYNTHESIS CODES

We computed the stellar structure for a large range of masses (from $M = 1$ to 6.5 $M_\odot$) and metallicities ($Z = 0.0001$, 0.004, 0.008, and 0.02) starting from the zero-age main sequence up through many thermal pulses during the AGB phase using the Mount Stromlo Stellar Structure Program (Wood & Zarro 1981; Frost & Lattanzio 1996). Mass loss is modeled on the AGB phase following the prescription of Vassiliadis & Wood (1993), which accounts for a final *superwind* phase. Using the prescription for unstable convective/radiative boundaries

described in detail by Lattanzio (1986), we find the TDU to occur self-consistently for masses above 2.25 $M_\odot$ at $Z = 0.02$, above 1.5 $M_\odot$ at $Z = 0.008$, above 1.25 $M_\odot$ at $Z = 0.004$, and for all the computed masses at $Z = 0.0001$. More details regarding these calculations can be found in Karakas (2003) and for the 3 $M_\odot$, $Z = 0.02$ model in Lugaro et al. (2003).

To calculate the nucleosynthesis in detail, we have used a postprocessing code that calculates abundance changes due to convective mixing and nuclear reactions (Cannon 1993). The stellar structure inputs, such as temperature, density, extent of convective zones, mixing length, and mixing velocity as functions of mass and model number, are taken from the stellar evolutionary computations. Between evolution models the postprocessing code creates its own mass mesh, resolving regions undergoing rapid changes in composition and using a combination of Lagrangian and non-Lagrangian points. Convective mixing is done time dependently, with no assumptions of instantaneous mixing. To model this, a "donor cell" scheme is adopted in which each nuclear species is stored as two variables representing two streams, one moving upward and one moving downward. At each mass shell matter flows freely from above or below with a certain degree of mixing and is also exchanged between adjacent cells, from one stream to the other.

Our nucleosynthesis network is based on 74 nuclear species, with 59 nuclei from neutrons and protons up to sulphur and another 14 nuclei near the iron group to allow neutron capture on iron seeds. There is also an additional "particle" g for counting the number of neutron captures occurring beyond ^{61}Ni, which simulates the *s*-process as neutron *sink*. The initial abundances in the postprocessing calculations are taken from Anders & Grevesse (1989). All proton, α-, and neutron captures and β-decays involving the species listed above are included in the nuclear network, summing up to 506 reactions. The bulk of reaction rates are from the REACLIB Data Tables of nuclear reaction rates based on the 1991 updated version of the compilation by Thielemann et al. (1986). The reaction rate table has been updated using the latest experimental results, which are listed in the Appendix. The reaction network is terminated by a neutron capture on ^{61}Ni followed by an ad hoc decay with $\lambda = 1\ \mathrm{s}^{-1}$ producing the particle represented by the symbol g: $^{61}\mathrm{Ni}(n,\ \gamma)^{62}\mathrm{Ni} \rightarrow {}^{61}\mathrm{Ni} + g$. Following the method of Jorissen & Arnould (1989), we model neutron captures on the missing nuclides by neutron sinks, meaning that the ^{34}S(n, γ)^{35}S and ^{61}Ni(n, γ)^{62}Ni reactions are given some averaged cross section values in order to represent all nuclei from ^{34}S to ^{55}Mn and from ^{61}Ni to ^{209}Bi, respectively (see also Lugaro et al. 2003; Herwig et al. 2003).

3. RESULTS FOR THE PRODUCTION OF FLUORINE

Our model predictions for the final ^{19}F intershell abundance are shown in Figure 1. Note that these calculations do not include a partial mixing zone. We find that the abundance of ^{19}F in the intershell is mostly dependent on two model features. The first is the temperature at the base of the convective pulse. As discussed by Mowlavi et al. (1996), this temperature determines the efficiencies of the rates of production and destruction of ^{19}F. Below $\simeq 2.2 \times 10^8$ K, ^{15}N is not efficiently converted into ^{19}F, while above $\simeq 2.6 \times 10^8$ K ^{19}F starts being destroyed by the $^{19}\mathrm{F}(\alpha, p)^{22}\mathrm{Ne}$ reaction. The stellar model of 3 $M_\odot$ and $Z = 0.02$ of Mowlavi et al. (1996) was shown to have pulse temperatures around the above range and hence to be the most efficient case for the production of fluorine with respect to the other two models presented by these authors: a 3 $M_\odot$, $Z = 0.001$ star and a 6 $M_\odot$, $Z = 0.02$ star. In the latter case proton captures at the hot base of the convective envelope (hot bottom burning) contribute to the destruction of fluorine. Also in our models the maximum abundance of ^{19}F in the He intershell at the end of the computed evolution is observed to occur at around 3 $M_\odot$, even though the temperatures are higher in our models, up to $\simeq 3 \times 10^8$ K.

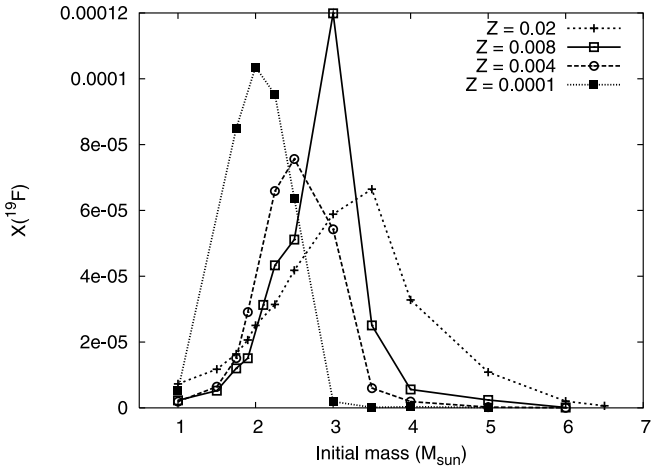

FIG. 1.—Mass fraction of ^{19}F in the He intershell after the last thermal pulse computed for each model. No partial mixing zone was included in these calculations.

The second parameter that determines the abundance of ^{19}F in the intershell is the amount of TDU. This is demonstrated by the fact that the maximum ^{19}F intershell abundance as a function of the stellar mass is about double in the case of $Z = 0.008$ what it is for $Z = 0.02$, which could appear at first surprising. In fact, one would expect to find a lower ^{19}F abundance at $Z = 0.008$ because the temperature in the convective pulse is slightly higher: in the $Z = 0.02$ case it ranges from 2.52×10^8 K in the 10th pulse to 3.05×10^8 K in the last pulse, while in the $Z = 0.008$ case the temperature is around 3×10^8 K in the last 10 pulses. Moreover, one would expect to find the ^{19}F abundance decreasing with the metallicity of the star since, when no partial mixing zone is included, its production depends on the amount of ^{13}C in the H ashes, which is of secondary nature, i.e., depends on the CNO abundances in the star. However, the abundance of ^{12}C in the envelope is a function of the amount of TDU. Since in our $Z = 0.008$ models the total mass dredged up by TDU is about twice that in the $Z = 0.02$ models, there is a strong effect on the production of ^{19}F due to the primary contribution to ^{13}C in the H-burning ashes coming from the dredged-up ^{12}C.

Furthermore, the reason why the abundance of ^{19}F decreases for masses lower than about 3 $M_\odot$ is mostly due to the lower TDU rather than the lower temperature in the convective pulse. This is demonstrated by the fact that the abundance of ^{15}N in all cases is insignificant with respect to that of ^{19}F, which means that the fraction of ^{15}N that has not burned into ^{19}F is unimportant. Out of all the models, a maximum value of 2.5×10^{-6} for the final ^{15}N intershell mass fraction is computed for the 1 $M_\odot$ $Z = 0.02$ star, compared to the final ^{19}F mass fraction of 7×10^{-6}.

When comparing with the previous results of Mowlavi et al. (1996), we find major differences due to two main reasons. The first is the fact that we have computed a much larger number of thermal pulses than Mowlavi et al. (1996). For example, for the stellar model of 6 $M_\odot$, $Z = 0.02$ we have computed 38 thermal

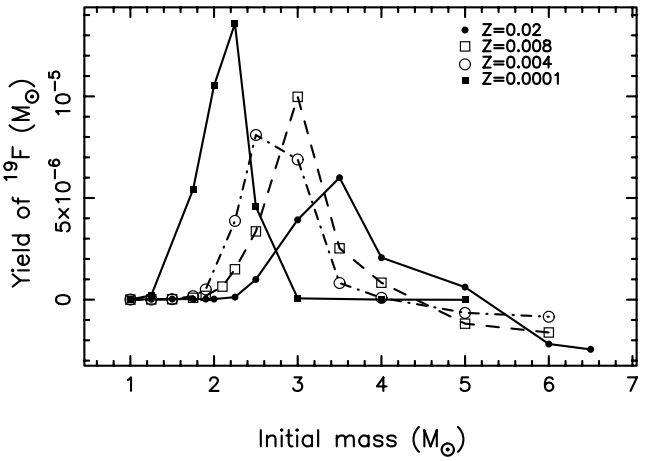

FIG. 2.—Yield of ^{19}F for each of the models presented in Fig. 1.

pulses, while Mowlavi et al. (1996) computed 11 thermal pulses. Hence, the temperature at the base of the last convective pulse, which increases with pulse number in AGB models, is higher in our calculations. In our 6 $M_\odot$, $Z = 0.02$ model the temperature reaches 3.5×10^8 K in the last thermal pulse, which is higher than the value of 2.8×10^8 K found by Mowlavi et al. (1996) simply because our last pulse represents a more advanced phase of the evolution. Hence, our final ^{19}F abundance in the He intershell for this case is more than an order of magnitude lower than that calculated by Mowlavi et al. (1996). On the other hand, because the TDU is self-consistently included in our calculations, we take into account the effect of the presence of primary ^{12}C in the envelope discussed above; thus, the final ^{19}F abundance for the 3 $M_\odot$, $Z = 0.02$ case in our calculation is about double that presented by Mowlavi et al. (1996). The same conclusion can be drawn when our results are compared with those of Forestini & Charbonnel (1997), which are very similar to the results from Mowlavi et al. (1996).

The production of fluorine in AGB stars is of interest also in the light of the Galactic chemical evolution. In Figure 2 and Table 1 we present yields for ^{19}F calculated for the different model shown in Figure 1. Yields are a direct function of the amount of TDU. They are calculated as net yields: $M = \int_0^\tau (X - X_0)(dM/dt)\,dt$, where τ is the total lifetime of the star, dM/dt is the mass-loss rate, and X and X_0 refer to the current and initial mass fraction of ^{19}F, respectively. The yield is positive if ^{19}F is produced and negative if it is destroyed.

TABLE 1

^{19}F YIELDS IN SOLAR MASSES FROM ALL THE COMPUTED STELLAR MODELS

M ($M_\odot$)	$Z = 0.02$	$Z = 0.008$	$Z = 0.004$	$Z = 0.0001$
1	3.65E−8	2.37E−9	9.45E−10	5.14E−9
1.25	1.59E−8	1.14E−8	6.23E−9	2.12E−7
1.50	2.51E−8	2.02E−8	2.29E−8	...
1.75	3.01E−8	9.01E−8	1.73E−7	5.43E−6
1.90	2.83E−8	1.87E−7	4.96E−7	...
2.00	2.72E−8	6.41E−7	...	1.05E−5
2.25	1.20E−7	1.49E−6	3.87E−6	1.36E−5
2.50	9.95E−7	3.36E−6	8.10E−6	4.56E−6
3.00	3.93E−6	9.98E−6	6.89E−6	6.20E−8
3.50	6.00E−6	2.52E−6	8.17E−7	...
4.00	2.07E−6	8.33E−7	8.90E−8	2.74E−9
5.00	6.12E−7	−1.18E−6	−6.50E−7	−6.94E−9
6.00	−2.18E−6	−1.62E−6	−8.41E−7	...
6.50	−2.45E−6	...	...	...

NOTE.—As in Fig. 2; no partial mixing zone included and reaction rates from the Appendix.

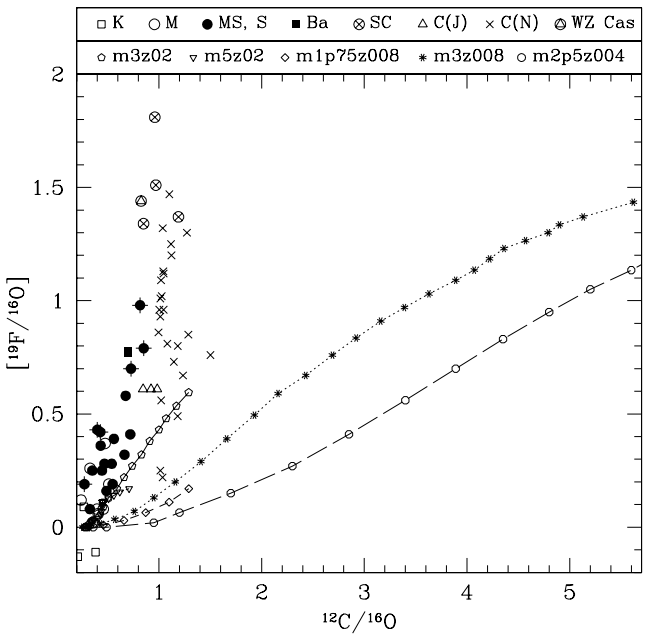

FIG. 3.—Comparison of fluorine abundances observed by Jorissen et al. (1992) and model predictions for selected stellar models: 3 and 5 $M_\odot$ with $Z = 0.02$; 1.75 and 3 $M_\odot$ with $Z = 0.008$; and 2.5 $M_\odot$ with $Z = 0.004$. Predictions are normalized in such a way that the initial ^{19}F abundance corresponds to the average F abundance observed in K and M stars, to which stellar data are normalized (see Jorissen et al. 1992). Each symbol on the prediction lines represents a TDU episode. Note that for the 2.5 $M_\odot$, $Z = 0.004$ model the final C/O = 11 and $[^{19}\mathrm{F}/^{16}\mathrm{O}] = 1.7$ are outside the range of the plot. Crossed MS, S symbols denote stars with large N excesses.

The ^{15}N yields are typically negative, decreasing from $\sim$0 for stars of 1 $M_\odot$ to $\simeq -2 \times 10^{-5}$ for stars of 6 $M_\odot$. This means that this isotope is destroyed in all the models, except those with $Z = 0.0001$ and mass higher than 2.25 $M_\odot$. The ^{15}N yield reaches a positive maximum of 4×10^{-6} for the highest mass model computed at this metallicity (5 $M_\odot$). This is due to a combination of different factors: (1) the temperature at the base of the convective envelope is as high as 9.7×10^7 K in this model, at which temperature the ^{14}N(p, γ)^{15}O reaction becomes as important as the ^{15}N(p, α)^{12}C reaction and ^{15}N can actually be produced by proton captures during hot bottom burning; (2) the abundance of ^{14}N is extremely high because of the operation of strong TDU and hot bottom burning; and (3) the initial ^{15}N abundance (X_0 in the formula above) is very low. The initial ^{19}F abundance is also very small; hence, the ^{19}F yields for this metallicity are less negative for masses above 4 $M_\odot$ compared to more metal-rich models of the same mass.

In Figure 3 we compare some selected model predictions with the observations by Jorissen et al. (1992). The metallicity of the observed stars ranges from about $Z = 0.006$ to about 0.04 with an average of 0.016. Hence, the 2.5 $M_\odot$, $Z = 0.004$ model has a metallicity too low to be considered to match the observations, and it is included in the figure only to illustrate the trend of our results with metallicity. The 3 $M_\odot$, $Z = 0.008$ model, which has the highest final ^{19}F abundance in the intershell, does not represent a good match to the stellar data. This is because the final C/O abundance in this model is 5.6, while the stellar data have C/O up to about 1.5. It follows that

since the large ^{19}F abundance in this model is a consequence of the large ^{12}C abundance in the envelope, we cannot take this model to explain the highest observed values. (We note, however, that stars with the high C/O ratio and high ^{19}F abundance produced by this model may in principle exist but may be obscured by their dusty envelopes.) It should also be considered that the observational data regarding SC stars require revision. For these stars it is difficult to derive reliable abundances because of the poor modeling of the atmospheres when $C/O \sim 1$.

The problem of matching the highest observed ^{19}F abundance could be overtaken by the inclusion of extra mixing processes at the base of the convective envelope, also referred to as cool bottom processing. This process occurs during the first red giant phase in stars with $M \leq 2.5\ M_{\odot}$ (see, e.g., Charbonnel 1995), as well as possibly during the AGB phase (Nollett et al. 2003), and results in a lower $^{12}C/^{13}C$ ratio than the standard models, as required by the observations. This type of extra mixing is described as the circulation of material from the base of the convective envelope into the thin radiative region located on top of the H-burning shell. Here the material is processed by proton captures and then carried back to the envelope, thus producing the signature of CNO processing at the stellar surface. Some of the MS and S stars with the highest [^{19}F/^{16}O] ratios for a given C/O ratio are also enhanced in N, up to 2.5 times the initial value (see Fig. 3 and discussion in Jorissen et al. 1992). This N enhancement could be due to cool bottom processing. If this process is at work, the surface $^{12}C/^{16}O$ ratio would appear to be lower than computed in our calculations. On the other hand, if the temperature at which the material is carried by cool bottom processing is lower than about 30 million degrees, at which value the $^{19}F(p, \alpha)^{16}O$ reaction is activated, then the ^{19}F abundance would be unchanged. This is because the ^{19}F production depends on the amount of ^{13}C in the H-burning ashes, which is a by-product of CNO cycling, and would not in principle be different if the CNO cycling occurs only in the H-burning shell or also at the base of the convective envelope via cool bottom processing. Then the theoretical curves of Figure 3 would be simply shifted to the left, making it easier to explain the observed ^{19}F abundances, together with the N excess. Note that WZ Cas is the only Li-rich star of the sample and has a very low $^{12}C/^{13}C$ ratio, a composition that is in agreement with this extra mixing. Cool bottom processing in the AGB phase is very uncertain, and detailed computations are not yet available. Since it has not been included in our computations, we cannot draw any quantitative conclusions on its possible effects.

Limiting the discussion to our current models, as shown in Figure 3, at $C/O \sim 1$ the 3 $M_{\odot}$, $Z = 0.02$ model shows a higher ^{19}F abundance in the envelope than the 3 $M_{\odot}$, $Z = 0.008$ model. In the 5 $M_{\odot}$, $Z = 0.02$ model, hot bottom burning is at work; hence, both ^{12}C and ^{19}F are destroyed. When comparing to previous calculations for the 3 $M_{\odot}$, $Z = 0.02$ model, we find that our final [^{19}F/^{16}O] ratio in the envelope is about 0.25 dex higher than that computed by Forestini & Charbonnel (1997) and Mowlavi et al. (1996) for the same $C/O \simeq 1.2$ ratio, which reflects our higher fluorine intershell abundance.

3.1. *The Impact of the Partial Mixing Zone*

To study the effect of the introduction of a partial mixing zone, we have included artificially in the postprocessing calculation a partial mixing zone at the end of each TDU episode. We have made the choice to include the partial mixing zone only when TDU occurs because during TDU a sharp discontinuity is produced between the convective envelope and the radiative intershell, which is a favorable condition for the occurrence of mixing (see, e.g., Iben & Renzini 1982). Since the question of the specific shape of the H profile and the mixing processes leading to the partial mixing zone is still open, we opted for a reasonable choice of the proton profile in which the number of protons decreases exponentially with the mass depth below the base of the convective envelope. We define as the partial mixing zone the region where the number of protons ranges from the envelope value to $X_p = 10^{-4}$. In this way about $\frac{1}{4}$ of the extent of the partial mixing zone has a number of protons between $X_p = 0.002$ and 0.02, corresponding to the efficient range for the production of ^{15}N (see Goriely & Mowlavi 2000). Note that Goriely & Mowlavi (2000) defined the partial mixing zone with the number of protons ranging from the envelope value to $X_p = 10^{-6}$ so that $\sim\frac{1}{6}$ of its extent corresponds to the efficient range for the production of ^{15}N. For the extent of the partial mixing zone we considered a value of $M_{\rm pmz} = 0.001\ M_{\odot}$, i.e., 1/15 of the mass of the last convective pulse for the 3 $M_{\odot}$, $Z = 0.02$ model. The dilution is higher for earlier pulses that have higher mass. This is a typical value adopted in the previous nucleosynthesis calculations (Gallino et al. 1998; Goriely & Mowlavi 2000).

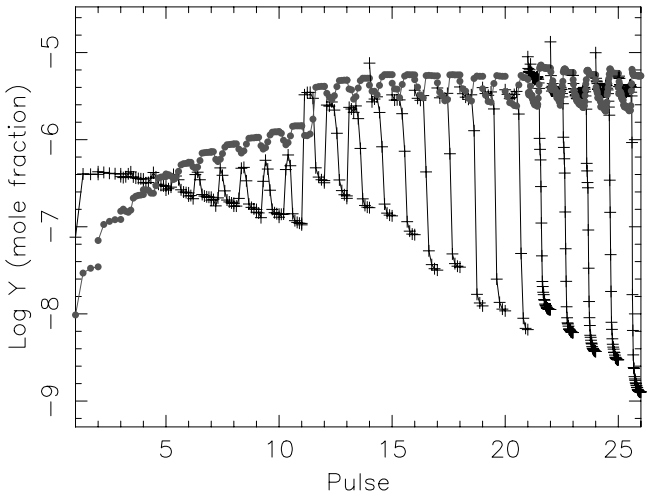

FIG. 4.—Abundance in number of ^{15}N (*crosses*) and ^{19}F (*filled circles*) in the He intershell as a function of the pulse number for the 3 $M_{\odot}$, $Z = 0.02$ model with a partial mixing zone of mass 0.001 $M_{\odot}$ included after each TDU episode, i.e., after the 10th thermal pulse. Abundances are plotted only during the time when the convective shell is present. The final abundances for each pulse are those corresponding to the pulse number tick mark in the *x*-axis.

In Figure 4 we show the abundance of ^{15}N and ^{19}F in the intershell during the period of convective instability following each thermal pulse for the 3 $M_{\odot}$, $Z = 0.02$ model. The final abundances in each pulse can be identified as those corresponding to the pulse number tick mark in the *x*-axis. At the beginning of a thermal pulse, while the convective instability is ingesting the H-burning ashes, ^{15}N is produced and its abundance sharply increases. At the same time the abundance of ^{19}F decreases because of the dilution of the intershell material with H-burning ashes where the abundance of ^{19}F is solar. Subsequently, ^{15}N is transformed into ^{19}F. In thermal pulses followed by TDU in our model, i.e., from the 10th thermal pulse onward, almost all ^{15}N is destroyed. The maximum temperature at the base of the 10th thermal pulse is equal to 2.52×10^8 K and ^{15}N is reduced to about 1/10 of its initial abundance in this pulse. In later pulses the temperature grows, reaching 3.05×10^8 K in the last thermal pulse so that

^{15}N is destroyed with even higher efficiency. In the very last few pulses also about 25% of the ^{19}F produced is destroyed. The effect of the partial mixing zone appears after the 11th thermal pulse where we observe large changes in the intershell abundances. For example, the amount of ^{15}N and ^{19}F suddenly increases: in the 11th thermal pulse the abundance of ^{19}F is about 2.5 times higher than that in the 10th thermal pulse. The final abundance of ^{19}F in the intershell is $\simeq$70% higher with respect to the case with no partial mixing zone included (shown in Fig. 1).

The extent in mass and the proton profile of the partial mixing zone are very uncertain parameters. Most studies that have self-consistently produced a partially mixed zone find that the extent in mass is smaller than the 0.001 $M_\odot$ value that we have used. The computed $M_{\rm pmz}$ is of the order of 10^{-6} $M_\odot$ with rotation, of 10^{-5} $M_\odot$ with overshoot (but depending on the free overshoot parameter!), and of 10^{-4} $M_\odot$ with gravitational waves. A partial mixing zone of larger extent, 5×10^{-4} $M_\odot$, was reported to result from semiconvection in a low-metallicity star (Hollowell & Iben 1988). On the other hand, previous nucleosynthesis studies have artificially considered partial mixing zones of extent up to 1/10 of the mass of the convective pulse. To check the uncertainty introduced by the extent of the partial mixing zone, we varied this parameter, thus computing three cases in total: one without the zone included, and the other two with the mass of the zone equal to $M_{\rm pmz} = 0.001$ and 0.002 $M_\odot$.

The results are presented in Figure 5 and show that the variation of the final abundance of ^{19}F in the envelope is up to a factor of $\sim$2 when the mass extent of the partial mixing zone is varied in the range described above. This could probably be considered as an upper limit for the uncertainty since a mass of $M_{\rm pmz} = 0.002$ $M_\odot$ is a large value to consider within the framework of the current models. A higher mass in fact would imply that the mixing process carrying protons into the He intershell region involves a large fraction of the intershell mass, which is not what the current studies indicate. We can only make a qualitative comparison with the results obtained by Goriely & Mowlavi (2000) since the stellar model considered and the computation procedure are different. Our case with $M_{\rm pmz} = 0.001$ $M_\odot$ and the case presented by Goriely & Mowlavi (2000) with $\lambda_{\rm pm} = M_{\rm pmz}/M_{\rm convective\ shell} = 0.1$ should have very similar values for the extent of the region where the production of ^{15}N is efficient in the partial mixing zone, corresponding to $\sim$1/60 of the total mass of the intershell. However, for this case the increase in the [^{19}F/^{16}O] ratio that we computed is more than 0.3 dex higher for the same C/O value around 1.2 than that presented in Figure 12 of Goriely & Mowlavi (2000). This is probably due to the fact that we have self-consistently taken the TDU into account.

The introduction of a partial mixing zone in some selected stellar models is illustrated in Table 2, where the ^{19}F yields are reported from computations performed without (col. [2]) and with (col. [3]) the inclusion of the partial mixing zone. In the 5 $M_\odot$ model the extent in mass of the intershell decreases from about 0.005 $M_\odot$ to about 0.001 $M_\odot$ at the end of the evolution. Hence for this model we have introduced a partial mixing zone of mass 0.001 $M_\odot$. Note also that in principle we do not know if and how the formation of the partial mixing zone is a function of the stellar properties. In the stellar models with mass $\simeq$3 $M_\odot$ the effect of the partial mixing zone introduces a factor of 2.6 uncertainty in the final yield; in the 5 $M_\odot$, $Z = 0.02$ model the uncertainty is of about a factor of 4; while in the low-mass model, 1.75 $M_\odot$, the uncertainty is of a factor of 14 in the final yield. However, as is discussed in § 4, this effect strongly depends on the uncertainties associated with the ^{14}C(α, γ)^{18}O reaction rate.

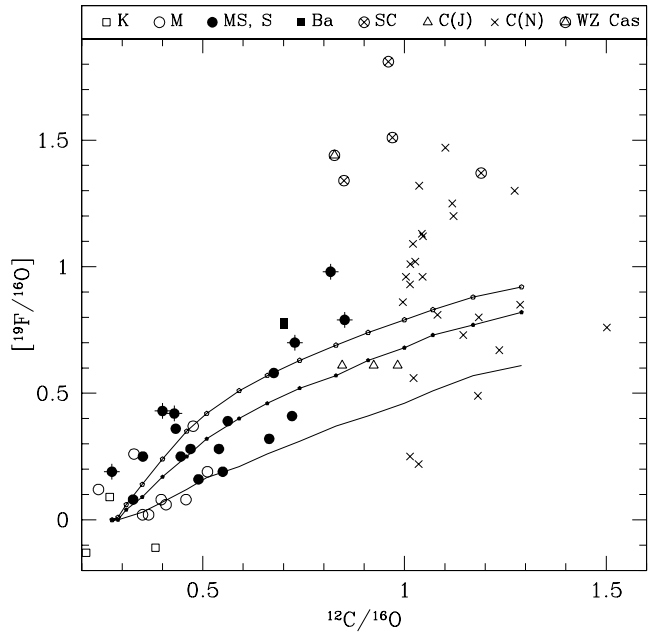

FIG. 5.—Comparison of fluorine abundances observed by Jorissen et al. (1992) and model predictions for the 3 $M_\odot$, $Z = 0.02$ model and different choices of the extent of the partial mixing zone. The bare line represents the cases in which no partial mixing zone is included. The lines accompanied by tiny filled and open circles refer to cases computed with a partial mixing zone with mass extent $M_{\rm pmz} = 0.001$ and 0.002 $M_\odot$, respectively. As in Fig. 3, crossed MS, S symbols denote stars with large N excesses, and predictions are normalized in such a way that the initial ^{19}F abundance corresponds to the average F abundance observed in K and M stars, to which stellar data are normalized (see Jorissen et al. 1992).

4. SUMMARY OF REACTION RATE STUDIES

There has been a considerable effort and improvement in the determination of the nuclear reaction rates over the last few years since the early ^{19}F nucleosynthesis studies. In particular, new measurements of key reactions such as ^{14}C(α, γ)^{18}O, ^{14}N(α, γ)^{18}F, ^{15}N(α, γ)^{19}F, and ^{18}O(α, γ)^{22}Ne provided new information on low-energy resonances that were ignored or only insufficiently included in previous simulations of ^{19}F nucleosynthesis. The results of all these studies are summarized and discussed in the following section. The main implication for the present study is that the new experimental results put a more stringent limit on the reaction rates and therefore reduce considerably the associated uncertainties compared to the uncertainties listed in the NACRE compilation (Angulo et al. 1999). There has not been much improvement in the ^{18}O(p, α)^{15}N rate, and there has been very little experimental effort in the study of ^{19}F(α, p)^{22}Ne. We therefore discuss the present nuclear physics–related uncertainties associated with both rates. For the latter case we also give a new reaction rate estimate based on experimental information and nuclear structure information on the compound nucleus ^{23}Na rather than on simple penetrability arguments.

4.1. *The Reaction Rate of* ^{13}C(α, n)^{16}O

For the ^{13}C(α, n)^{16}O reaction, we have used the rate from Drotleff et al. (1993) and Denker et al. (1995), which is about

TABLE 2
^{19}F Yields in Solar Masses from Selected Stellar Models

Rates (1)	Standard[a] (2)	Standard[a] (3)	Recommended[b] (4)	Upper[c] (5)	Lower[d] (6)
M_{pmz} ($M_\odot$).....	0	0.002[e]	0.002[e]	0.002[e]	0.002[e]
3, 0.02	3.93E−6	1.01E−5	6.49E−6	7.10E−6	4.78E−6
5, 0.02	6.12E−7	2.46E−6	3.21E−6	4.06E−6	6.18E−7
1.75, 0.008	9.01E−8	1.23E−6	5.39E−7	5.96E−7	4.37E−7
3, 0.008	9.98E−6	2.23E−5	1.94E−5	2.09E−5	1.36E−5
2.5, 0.004	8.10E−6	1.96E−5	1.60E−5	1.69E−5	1.21E−5

Notes.—Since each model run takes at least one CPU day, it is unfeasible to repeat all the calculations presented in § 3. More calculations will be performed under specific requests.

[a] As listed in the Appendix.

[b] As described in § 4, specifically: ^{14}N(α, γ)^{18}F from Görres et al. (2000), ^{18}O(α, γ)^{22}Ne from Dababneh et al. (2003), and our recommended values for ^{14}C(α, γ)^{18}O and ^{19}F(α, p)^{22}Ne.

[c] Upper limit for the ^{14}C(α, γ)^{18}O rate and lower limit for the ^{19}F(α, p)^{22}Ne rate (§ 4) to obtain the upper limit for the yields.

[d] Lower limit for the ^{14}C(α, γ)^{18}O rate and upper limit for the ^{19}F(α, p)^{22}Ne rate (§ 4) to obtain the lower limit for the yields.

[e] But 0.001 in the 5, 0.02 models.

50% lower than the rate recommended by NACRE in the temperature range of interest. Recent ^{13}C(^{6}Li, d) α-transfer studies (Kubono et al. 2003) suggest a very small spectroscopic factor of $S_\alpha = 0.01$ for the subthreshold state at 6.356 MeV. This indicates that the high-energy tail for this state is negligible for the reaction rate, in agreement with the present lower limit. However, a detailed reanalysis by Keeley et al. (2003) of the transfer data leads to significantly different results for the spectroscopic factor of the subthreshold state $S_\alpha = 0.2$, which would imply good agreement with the value used in this paper. This situation requires further experimental and theoretical study. A reevaluation of the rate based on new experimental results has been performed by Heil (2002) and will be published in a forthcoming paper. The choice of the ^{13}C(α, n)^{16}O reaction within the current possibilities only slightly affects the production of ^{15}N and ^{19}F. Using the rate by Denker et al. (1995) in the 3 $M_\odot$, $Z = 0.02$ model with a partial mixing zone of mass 0.002 $M_\odot$ gives an 8% increase in the final surface ^{19}F with respect to the calculation done using the NACRE rate. This result can be understood when the ^{13}C(α, n)^{16}O rate is compared to the ^{14}C(α, γ)^{18}O reaction, as discussed in the next subsection.

4.2. *The Reaction Rate of* ^{14}C(α, γ)^{18}O

The reaction ^{14}C(α, γ)^{18}O has been studied experimentally in the energy range of 1.13–2.33 MeV near the neutron threshold in the compound nucleus ^{18}O by Görres et al. (1992). The reaction rate is dominated at higher temperatures by the direct capture and the single strong 4^+ resonance at center-of-mass energy $E_{cm} = 0.89$ MeV. Toward lower temperatures, which are of importance for He shell burning in AGB stars, important contributions may come from the 3^- resonance at $E_{cm} = 0.176$ MeV ($E_x = 6.404$ MeV) and a 1^- subthreshold state at $E_x = 6.198$ MeV. It has been shown in detailed cluster model simulations that neither one of the two levels is characterized by a pronounced α cluster structure (Descouvemont & Baye 1985). The strengths of these two contributions are unknown and have been estimated by Buchmann et al. (1988), adopting an α spectroscopic factor of $\Theta^2_\alpha = 0.02$ and 0.06 for the 6.404 and 6.198 MeV states, respectively, for determining the 0.176 MeV resonance strength and the cross section of the high-energy tail of the subthreshold state. While the value for the 6.404 MeV state is in agreement with the results of a ^{14}C(^{6}Li, d)^{18}O α-transfer experiment (Cunsolo et al. 1981), the value for the 6.2 MeV state appears rather large since the corresponding α-transfer was not observed. This reflects the lack of appreciable α-strength in agreement with the theoretical predictions. We therefore adopted an upper limit for the spectroscopic factor of this resonance of $\Theta^2_\alpha = 0.02$. The upper limit for the reaction rate is based on the experimental data (Görres et al. 1992) plus the low-energy resonance contributions calculated from the upper limit for the α spectroscopic factor. For the recommended reaction rate we adopted a considerably smaller spectroscopic factor $\Theta^2_\alpha = 0.01$ for calculating the $\omega\gamma$ strength of the 0.176 MeV resonance. In this we followed the recommendations by Funck & Langanke (1989). The lower limit of the reaction rate neglects the contribution of this resonance altogether and corresponds directly to the experimental results (Görres et al. 1992). It should be noted, however, that the uncertainty for the resonance strength and therefore its contribution to the reaction rate is up to 5 orders of magnitude as shown in Figure 6.

The ^{14}C(α, γ)^{18}O reaction can be activated together with the ^{13}C(α, n)^{16}O reaction during the interpulse period, in both the partial mixing zone and the deepest layer of the region composed by H-burning ashes, when ^{14}N(n, p)^{14}C occurs, and it represents the main path to the production of ^{18}O and subsequently of ^{15}N. The importance of the nucleosynthesis of ^{15}N during the interpulse periods is very much governed by the choice of the rate of the ^{14}C(α, γ)^{18}O reaction. The closer, or higher, this rate is to that of the ^{13}C(α, n)^{16}O reaction, the more efficient is the production of ^{15}N because ^{18}O and protons are produced together. The effect of the partial mixing zone and hence the uncertainties related to it are in fact much less important when using our recommended rate, since in the temperature range of interest our rate is more than an order of magnitude lower than our standard rate from NETGEN (Jorissen & Goriely 2001), which was also used in the previous study by Goriely & Mowlavi (2000; see Fig. 7). At the temperature of interest the NETGEN rate is based on previous theoretical studies by Funck & Langanke (1989) and Hashimoto et al. (1986). When using our recommended rate to compute the 3 $M_\odot$, $Z = 0.02$ model with a partial mixing zone of mass 0.002 $M_\odot$, the final [^{19}F/^{16}O] is the same as that computed without the partial mixing zone within 10%.

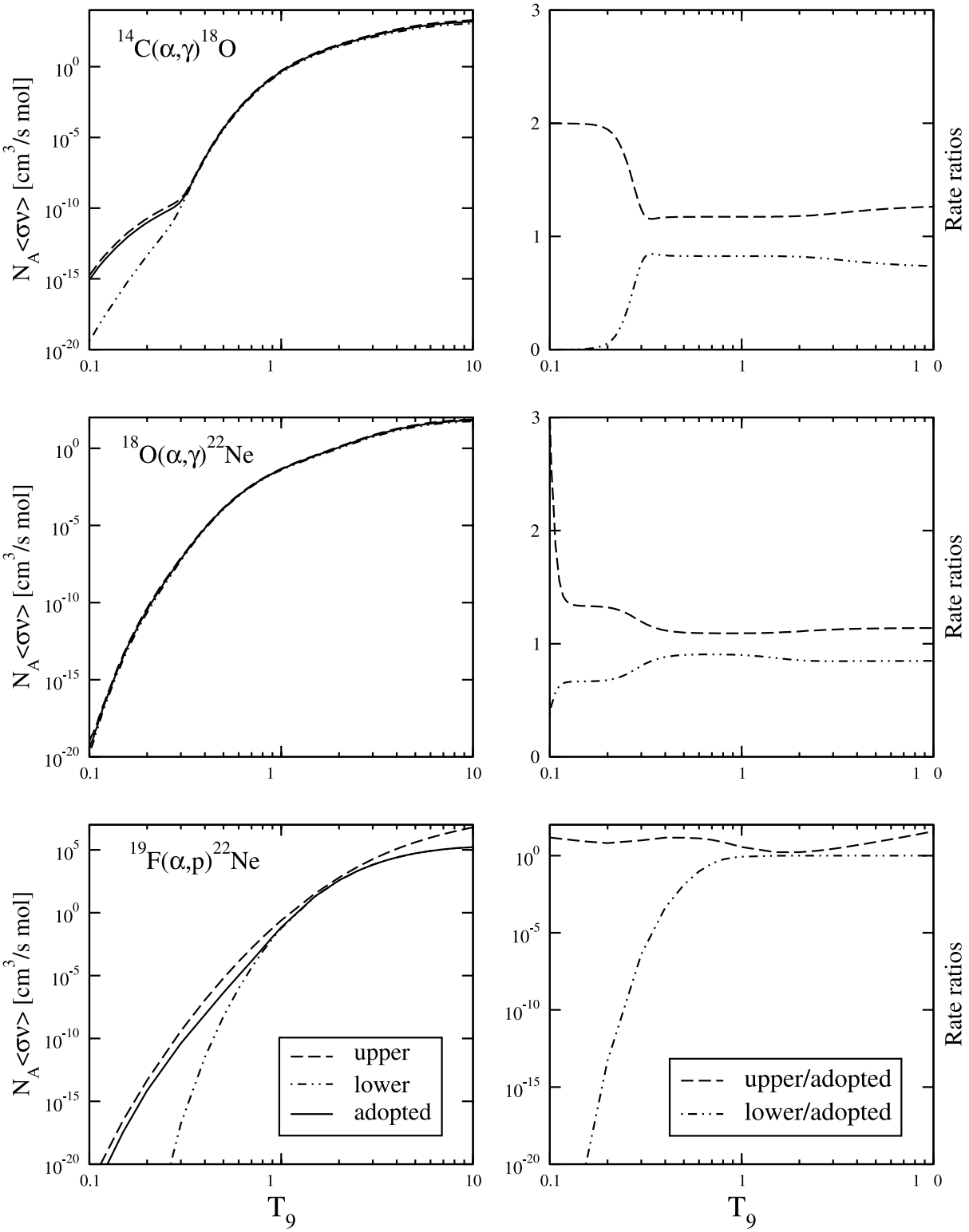

FIG. 6.—Recommended lower and upper limits for the rates of the ^{14}C(α, γ)^{18}O, ^{18}O(α, γ)^{22}Ne, and ^{19}F(α, p)^{22}Ne reactions.

4.3. *The Reaction Rate of* ^{14}N(α, γ)^{18}F

The low-energy resonances in ^{14}N(α, γ)^{18}F have recently successfully been measured by Görres et al. (2000). Previous uncertainties about the strengths of these low-energy resonances were removed. Because of these results, the reaction rate is reduced by about a factor of 3 compared to NACRE.

The ^{14}N(α, γ)^{18}F reaction is inefficient at the temperature of neutron release in the partial mixing zone while it is activated in the convective pulse. Hence, its rate only affects the production of ^{19}F in the pulse. Using the new rate by Görres et al. (2000) with respect to the rate by Caughlan & Fowler (1988, hereafter CF88), which is the same as NACRE within 10%, only very marginally changes the production of ^{19}F. For

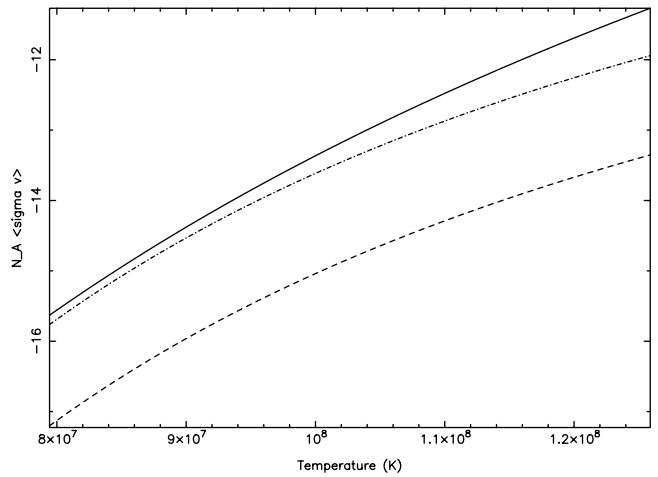

FIG. 7.—Rate for the $^{13}C(\alpha, n)^{16}O$ reaction (Drotleff et al. 1993; Denker et al. 1995; *solid line*) compared to two different choices for the $^{14}C(\alpha, \gamma)^{18}O$ reaction rate: NETGEN (*dot-dashed line*) and our recommended rate (*dashed line*) in the range of temperature at which the $^{13}C(\alpha, n)^{16}O$ reaction is activated in the ^{13}C pocket.

example, in the 3 $M_\odot$ $Z = 0.02$ model with a partial mixing zone of mass 0.002 $M_\odot$ the final abundance in the envelope is increased by about 5% using the new rate.

4.4. *The Reaction Rate of* $^{15}N(\alpha, \gamma)^{19}F$

The reaction rate of $^{15}N(\alpha, \gamma)^{19}F$ was taken from NACRE. The rate is dominated by the contribution of three low-energy resonances. The resonance strengths are based on the analysis of de Oliveira et al. (1996). It should be noted, however, that there were several recent experimental studies that point toward a significantly higher reaction rate. De Oliveira et al. (1997) already suggested higher resonance strengths than given in their earlier paper. Direct α-capture measurements of the two higher energy states by Wilmes et al. (2002) also indicate higher strengths. A recent indirect α-transfer analysis to the three resonance levels by Fortune & Lacaze (2003) does suggest even higher values for the resonance strengths. Altogether the reaction rate of $^{15}N(\alpha, \gamma)^{19}F$ used in this work might be underestimated by a factor of 5.

Using the reaction rate by CF88 for $^{15}N(\alpha, \gamma)^{19}F$, which is about 50 times higher with respect to the new estimate by de Oliveira et al. (1996), did not change the results in the 3 $M_\odot$ $Z = 0.02$ model with a partial mixing zone of mass 0.002 $M_\odot$. The final ^{19}F abundance in the envelope increased by a few percent only. This is because the temperature in the thermal pulses is high enough that in any case all ^{15}N is transformed in ^{19}F, as shown in Figure 4. This point was discussed by de Oliveira et al. (1996), who showed that at temperatures higher than $\simeq 2.6 \times 10^8$ K, such as those in our thermal pulses followed by TDU, the difference between using the two rates is minimal. Hence, even if the final rate will actually be higher than the latest estimate, this will not make a difference to the final results. A maximum increase of 35% in the final ^{19}F intershell abundance would occur in the case of the 1 $M_\odot$, $Z = 0.02$ model, assuming that all ^{15}N would burn into ^{19}F (see § 3).

4.5. *The Reaction Rate of* $^{15}N(p, \alpha)^{12}C$

The $^{15}N(p, \alpha)^{12}C$ reaction has been investigated by Schardt et al. (1952), Zyskind & Parker (1979), and more recently by Redder et al. (1982) at $E_p(\text{lab}) = 78-810$ keV. These results were summarized and compiled by NACRE. The reaction rate at $T_9 \sim 0.2$ is dominated by the $J^\pi = 1^-$ resonance at $E_p = 334$ keV. However, contributions from three other resonances at 1027, 1639, and 2985 keV have been included as well. Using the NACRE rate, which is up to a factor of 2 higher than the rate by CF88, we obtain a small decrease of $\simeq 8\%$ in the final surface abundance of ^{19}F in the 3 $M_\odot$, $Z = 0.02$ model with a partial mixing zone of mass 0.002 $M_\odot$.

4.6. *The Reaction Rate of* $^{18}O(\alpha, \gamma)^{22}Ne$

The $^{18}O(\alpha, \gamma)^{22}Ne$ reaction is of interest for the discussion of ^{19}F production in AGB stars since it competes with the $^{18}O(p, \alpha)^{15}N$ process. A strong rate might lead to a reduction in ^{19}F production. The reaction rate of $^{18}O(\alpha, \gamma)^{22}Ne$ has been last summarized and discussed by Käppeler et al. (1994) and by the NACRE compilation. The main uncertainties result from the possible contributions of low-energy resonances that have been estimated on the basis of α-transfer measurements by Giesen et al. (1994). A recent experimental study of $^{18}O(\alpha, \gamma)^{22}Ne$ by Dababneh et al. (2003) led to the first successful direct measurement of the postulated low-energy resonances at 470 and 566 keV, thus reducing to 33% the previous uncertainty of about a factor of 30 given by NACRE at the temperature of interest, which was given by taking the previously available experimental upper limit for the 470 keV resonance strength (Giesen et al. 1994). The new rate is shown in Figure 6. Not measured still is the 218 keV resonance, which is expected to dominate the rate at temperatures of $T \leq 0.1$ GK, well below the temperature in typical He-burning conditions. The resulting reaction rate is in very good agreement with the previous estimate by Käppeler et al. (1994), which was used for our calculations of ^{19}F production.

4.7. *The Reaction Rate of* $^{18}O(p, \alpha)^{15}N$

The reaction $^{18}O(p, \alpha)^{15}N$ provides a major link for the production process of ^{19}F. The reaction cross section has been measured by Lorenz-Wirzba et al. (1979) down to energies of $\approx$70 keV. Possible contributions of low energy near threshold resonances were determined by Wiescher & Kettner (1982) and Champagne & Pitt (1986) using direct capture and single-particle transfer reaction techniques. These results were compiled and summarized by NACRE. The reaction rate uncertainties are less than an order of magnitude, as well as less than a factor of 2 in the range of temperature of interest, and are mainly related to uncertainties in the reasonably well studied single-particle structure of these threshold resonance states. The NACRE rate is the same within 10% of the rate given by CF88. Hence, we do not currently have major uncertainties on the ^{19}F production coming from this rate.

4.8. *The Reaction Rate of* $^{19}F(\alpha, p)^{22}Ne$

The reaction rate of $^{19}F(\alpha, p)^{22}Ne$ is one of the most important input parameters for a reliable analysis of ^{19}F nucleosynthesis at AGB stars. However, there is very little experimental data available for the $^{19}F(\alpha, p)^{22}Ne$ reaction cross section at low energies. Experiments were limited to the higher energy range above $E_\alpha = 1.3$ MeV (Kuperus 1965). CF88 suggested a rate that is based on a simple barrier penetration model previously used by Wagoner (1969). This reaction rate is in reasonable agreement with more recent Hauser-Feshbach estimates assuming a high level density (see Thielemann et al. 1986) and has therefore been used in most of the previous

nucleosynthesis simulations. The applicability of the Hauser-Feshbach model, however, depends critically on the level density in the compound nucleus system (Rauscher et al. 1997). We analyzed the level density in the compound nucleus ^{23}Na above the α-threshold of $Q_\alpha = 10.469$ MeV as compiled by Endt & van der Leun (1978) and Endt (1990). The typical level density is ≈ 0.02 keV^{-1}. This level density is confirmed directly for the ^{19}F(α, p) reaction channel by direct studies from Kuperus (1965) at resonance energies above 1.5 MeV and further confirmed by as yet unpublished low-energy ^{19}F(α, p) resonance measurements of C. Ugalde (2004, unpublished). This low resonance density translates into an averaged level spacing of $D \approx 50$ keV, which is considerably larger than the average resonance width of $\Gamma \approx 8$ keV in this excitation range. Based on these estimates, the requirement of $D \leq \Gamma$ for the applicability of the Hauser-Feshbach approach (Rauscher et al. 1997) is not fulfilled. The reaction rate for ^{19}F$(\alpha, p)^{22}$Ne therefore needs to be calculated from determining the strengths $\omega\gamma$ for the single resonances,

$$\omega\gamma = \frac{(2J+1)}{2}\frac{\Gamma_\alpha \Gamma_p}{\Gamma_{\rm tot}}. \quad (1)$$

We estimated the α partial width Γ_α using a simple WKB approximation with an average α spectroscopic factor of $C^2 S_\alpha = 0.001$. This average spectroscopic factor was determined from determining the average α-strength distribution from the strengths of observed α-capture resonances at higher energies (Kuperus 1965) and from the α spectroscopic strengths of bound states in ^{23}Na (Fortune et al. 1978). The total widths $\Gamma_{\rm tot}$ of the levels correspond in all cases to the proton partial widths Γ_p; therefore, the resonance strength depends entirely on the spin J and the α partial width Γ_α of the resonance levels. For the higher energy range $E_\alpha \geq 1.5$ MeV we used directly the experimentally determined resonance strengths by Kuperus (1965). The resulting reaction rate is shown in Figure 6 and deviates considerably from the Hauser-Feshbach prediction; in the temperature range of intershell He burning it is more than 1 order of magnitude smaller than predicted in the Hauser-Feshbach estimate. The possibility of "missing strength" in as yet unobserved resonances seems unlikely as shown by the previous ^{19}F(α, p) studies but cannot be completely excluded. However, a substantial increase in the reaction rate would rather be associated with a large α-strength of the low-energy unbound states in ^{23}Na. Therefore, an experimental confirmation of the here predicted resonance strength distribution is desirable for a wide energy range.

Using our new recommended rate, for example, in the 3 $M_\odot$, $Z = 0.02$ model, the final [^{19}F/^{16}O] is 0.1 dex higher than in the case computed using the CF88 rate. The effect of this rate and its uncertainties is larger for higher mass models, where the temperature is higher and the ^{19}F$(\alpha, p)^{22}$Ne is more activated.

4.9. *Other Rates of Interest*

The ^{13}C$(p, \gamma)^{14}$N reaction is of interest regarding the formation of ^{13}C in the partial mixing zone. The experimental rate by King et al. (1994) is 1.29 times higher than the rate given by CF88 at the temperature of interest, and the revision by NACRE, which we used, gives a rate 1.20 times higher than CF88. A higher rate will result in a lower ^{13}C abundance and a lower neutron flux during the interpulse period. Calculations for the 3 $M_\odot$, $Z = 0.02$ model showed that the difference of 10% less between NACRE and the rate by King et al. (1994) yields a 5% increase in the ^{15}N produced during the interpulse and a 6% increase in the final surface ^{19}F. We also checked that within the current uncertainties of the ^{14}N$(n, p)^{14}$C rate ($\simeq$10%; Gledenov et al. 1995) and the less important ^{14}N$(n, \gamma)^{15}$N rate (uncertainties of a factor of about 2.5; Beer et al. 1992), the final results do not change.

5. DISCUSSION AND CONCLUSIONS

Using the new rates presented in the previous section, in particular for the ^{14}C$(\alpha, \gamma)^{18}$O and the ^{19}F$(\alpha, p)^{22}$Ne reactions, we have calculated recommended upper and lower limits for the production of ^{19}F in selected stellar models (Table 2). The runs computed with no inclusion of the partial mixing zone (col. [2]) can be considered, within our models, as absolute lower limits for the ^{19}F yields. The runs computed with the recommended rates and including the partial mixing zone (col. [4]) show a decrease in the yield with respect to the same runs computed with the "standard" rates (col. [3]), except for the 5 $M_\odot$, $Z = 0.02$ model. This decrease is due to our estimate of the ^{14}C$(\alpha, \gamma)^{18}$O reaction, which makes the contribution of the partial mixing zone to the production of ^{19}F much less significant. In the case of the 5 $M_\odot$, $Z = 0.02$ model the yield increases by a factor of 1.3 owing to the fact that the temperatures in this intermediate-mass model are higher than in the other models and hence the effect of our lower estimate for the ^{19}F$(\alpha, p)^{22}$Ne rate is more important. The overall uncertainties in the ^{19}F production due to the uncertainties in the reaction rates are about 50% in the stellar models with mass $\simeq 3$ $M_\odot$ and about 40% in stellar models of lower mass. For the 5 $M_\odot$, $Z = 0.02$ stellar model the uncertainties are about a factor of 7, as a result of the large uncertainties of the ^{19}F$(\alpha, p)^{22}$Ne rate.

The ^{19}F$(\alpha, p)^{22}$Ne reaction rate also influences the production of fluorine in the winds of Wolf-Rayet stars; hence, models of this type of stars should also be revised to test the effect of our revised rate and its uncertainties. It is also important to note that our estimated lower limit for the ^{19}F$(\alpha, p)^{22}$Ne rate is about 4 orders of magnitude lower than the ^{22}Ne$(\alpha, n)^{25}$Mg reaction rate. In this case the ^{19}F$(n, \gamma)^{20}$F reaction has to be taken into account as a possible destruction channel for ^{19}F when a significant neutron flux is released in the convective pulses of AGB stars and in Wolf-Rayet stars by the ^{22}Ne$(\alpha, n)^{25}$Mg reaction.

For the 3 $M_\odot$, $Z = 0.02$ model surface abundances are also shown in Figure 8 for a given choice of the partial mixing zone with $M_{\rm pmz} = 0.002$ $M_\odot$. With the new estimate for the ^{14}C$(\alpha, \gamma)^{18}$O rate the contribution of the partial mixing zone is diminished, making this uncertain parameter less important. In particular, in the lower limit case, the resulting [^{19}F/^{16}O] ratio is the same within 10% as computed without including the partial mixing zone (compare to Fig. 5). In none of the cases we calculated could the highest [^{19}F/^{16}O] values observed be reproduced. As discussed in § 3, this problem should be reviewed with the inclusion in future calculations of extra mixing processes (cool bottom processing) at the base of the convective envelope.

Future work should also improve our knowledge of the formation and the nucleosynthesis in the partial mixing zone. One hypothesis is that rotation can play a role in varying the efficiency of the production of ^{19}F and of the *s*-process elements (Herwig et al. 2003). It will be of much interest to analyze the effects of this hypothesis on the correlation between fluorine and the *s*-process elements and to revise the

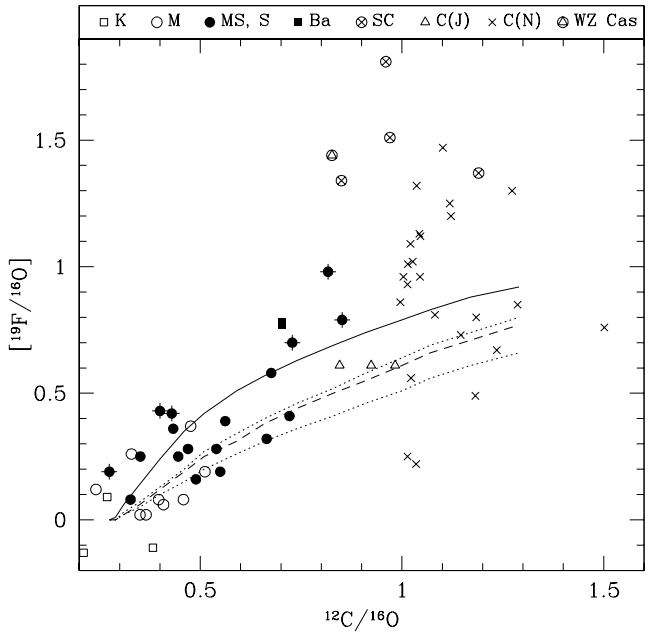

FIG. 8.—Comparison of fluorine abundances observed by Jorissen et al. (1992) and model predictions for the 3 $M_{\odot}$, $Z = 0.02$ model and $M_{\rm pmz} = 0.002\ M_{\odot}$ and different choices of the rate of the reactions involved as described in Table 2: "standard" (*solid line*), "recommended" (*short-dashed line*), and lower and upper limit (*dotted lines*). As in Fig. 3, crossed MS, S symbols denote stars with large N excesses, and predictions are normalized in such a way that the initial ^{19}F abundance corresponds to the average F abundance observed in K and M stars, to which stellar data are normalized (see Jorissen et al. 1992).

available observational data. Using data for carbon stars from Utsumi (1985), it appeared that these two quantities were correlated in AGB stars; however, using more recent and precise data from Abia et al. (2002), this correlation does not seem to appear anymore.

Another problem is related to C(J) stars. It is still unknown if these stars actually belong to the AGB group or if they are in some other phase of the evolution. Moreover, it appears that their [^{19}F/^{16}O] ratios around 0.6 are due to a low abundance of ^{16}O rather than a high abundance of ^{19}F. Finally, the observational data regarding SC stars should be updated using more recent atmospheric models.

M. L. deeply appreciates the hospitality and support extended to her by Michael Wiescher, Joachim Görres, and Claudio Ugalde during a visit to Notre Dame University, as well as the hospitality received by John Lattanzio and Amanda Karakas during a visit to Monash University. We thank Roberto Gallino, Enrico Arnone, Stefano Masera, and Richard Stancliffe for discussion and help. The manuscript was much extended and improved following strong criticisms by the anonymous referee. This work was supported by the Australian Research Council and the Australian Partnership for Advanced Computing. Computational resources used for this study were also partly funded by the Canada Foundation for Innovation (CFI) and the Nova Scotia Research and Innovation Trust (NSRIT) Fund.

APPENDIX

DETAILS OF THE REACTION RATES USED IN THE REFERENCE CASE

References for proton, α-, and neutron captures that we have used in the nucleosynthesis calculations are presented in Tables 3, 4, and 5, respectively. All of the reactions not listed in the tables are taken from the REACLIB Data Tables (version 1991).

TABLE 3
PROTON CAPTURES

Reaction	References
^{7}Be(p, γ)^{8}B	Hammache et al. (1998)
^{13}C(p, γ)^{14}N	Angulo et al. (1999)
^{14}C(p, γ)^{15}N	Wiescher et al. (1990)
^{13}N(p, γ)^{14}O	Decrock et al. (1993)
^{17}O(p, γ)^{18}F	Blackmon et al. (1995), Landré et al. (1990)
^{17}O(p, α)^{14}N	Blackmon et al. (1995), Landré et al. (1990)
^{18}F(p, γ)^{19}Ne	Utku et al. (1998)
^{18}F(p, α)^{15}O	Utku et al. (1998)
^{21}Ne(p, γ)^{22}Na	El Eid & Champagne (1995)
^{22}Ne(p, γ)^{23}Na	El Eid & Champagne (1995)
^{22}Na(p, γ)^{23}Mg	Stegmüller et al. (1996), Schmidt et al. (1995), Seuthe et al. (1990)
^{23}Na(p, γ)^{24}Mg	El Eid & Champagne (1995)
^{23}Na(p, α)^{20}Ne	El Eid & Champagne (1995)
^{24}Mg(p, γ)^{25}Al	Powell et al. (1999)
^{25}Mg(p, γ)^{26}Al$^{g/i}$	Iliadis et al. (1996), Iliadis et al. (1990)
^{26}Mg(p, γ)^{27}Al	Iliadis et al. (1990)
^{26}Al^{g}(p, γ)^{27}Si	Champagne et al. (1993), Vogelaar et al. (1996)
^{27}Al(p, γ)^{28}Si	Iliadis et al. (1990), Timmermann et al. (1988)
^{27}Al(p, α)^{24}Mg	Timmermann et al. (1988), Champagne et al. (1988)
^{28}Si(p, γ)^{29}P	Graff et al. (1990)

TABLE 4

α-Captures

Reaction	References
$^{13}C(\alpha, n)^{16}O$	Drotleff et al. (1993), Denker et al. (1995)
$^{14}C(\alpha, \gamma)^{18}O$	Jorissen & Goriely (2001)
$^{15}N(\alpha, \gamma)^{19}F$	de Oliveira et al. (1996)
$^{17}O(\alpha, n)^{20}Ne$	Denker et al. (1995)
$^{18}O(\alpha, \gamma)^{22}Ne$	Käppeler et al. (1994), Giesen et al. (1994)
$^{18}O(\alpha, n)^{21}Ne$	Denker et al. (1995)
$^{21}Ne(\alpha, n)^{24}Mg$	Denker et al. (1995)
$^{22}Ne(\alpha, \gamma)^{26}Mg$[a]	Käppeler et al. (1994)
$^{22}Ne(\alpha, n)^{25}Mg$[a]	Drotleff et al. (1993), (1995)

[a] The elusive resonance at 633 keV has not been included.

TABLE 5

Neutron Captures

Reaction[a]	References
$^{12}C(n, \gamma)^{13}C$	Kikuchi et al. (1998)
$^{13}C(n, \gamma)^{14}C$	Raman et al. (1990); A. Mengoni (1998, private communication)
$^{14}N(n, p)^{14}C$	Gledenov et al. (1995)
$^{16}O(n, \gamma)^{17}O$	Igashira et al. (1995)
$^{18}O(n, \gamma)^{19}O$	Meissner et al. (1996)
$^{26}Al^{g}(n, p)^{26}Mg$	Koehler et al. (1997)
$^{26}Al^{g}(n, \alpha)^{26}Mg$	Koehler et al. (1997), Skelton et al. (1987)
$^{33}S(n, \alpha)^{30}Si$	Schatz et al. (1995)

[a] The (n, γ) reactions on stable nuclei not listed here are all from Beer et al. (1992). Among those, the $^{28}Si(n, \gamma)$ cross section has been renormalized to the value given by Bao & Käppeler (1987) following H. Beer (1990, private communication).

REFERENCES

Abia, C., Domínguez, I., Gallino, R., Busso, M., Masera, S., Straniero, O., de Laverny, P., & Plez, B. 2002, ApJ, 579, 817
Anders, E., & Grevesse, N. 1989, Geochim. Cosmochim. Acta, 53, 197
Angulo, C., et al. 1999, Nucl. Phys. A, 656, 3
Bao, Z. Y., & Käppeler, F. 1987, At. Data Nucl. Data Tables, 36, 411
Beer, H., Voss, F., & Winters, R. R. 1992, ApJS, 80, 403
Blackmon, J. C., Champagne, A. E., Hofstee, M. A., Smith, M. S., Downing, R. G., & Lamaze, G. P. 1995, Phys. Rev. Lett., 74, 2642
Buchmann, L., D'Auria, J. M., & McCorquodale, P. 1988, ApJ, 324, 953
Cannon, R. C. 1993, MNRAS, 263, 817
Caughlan, G. R., & Fowler, W. A. 1988, At. Data Nucl. Data Tables, 40, 283 (CF88)
Champagne, A. E., Brown, B. A., & Sherr, R. 1993, Nucl. Phys. A, 556, 123
Champagne, A. E., Cella, C. H., Kouzes, R. T., Lowry, M. M., Magnus, P. V., Smith, M. S., & Mao, Z. Q. 1988, Nucl. Phys. A, 487, 433
Champagne, A. E., & Pitt, M. L. 1986, Nucl. Phys. A, 457, 367
Charbonnel, C. 1995, ApJ, 453, L41
Cunha, K., Smith, V. V., Lambert, D. L., & Hinkle, K. H. 2003, AJ, 126, 1305
Cunsolo, A., Foti, A., Immè, G., Pappalardo, G., Raciti, G., & Saunier, N. 1981, Phys. Rev. C, 24, 476
Dababneh, S., Heil, M., Käppeler, F., Görres, J., Wiescher, M., Reifarth, R., & Leiste, H. 2003, Phys. Rev. C, 68, 025801
Decrock, P., et al. 1993, Phys. Rev. C, 48, 042057
Denissenkov, P. A., & Tout, C. A. 2003, MNRAS, 340, 722
Denker, A., et al. 1995, in AIP Conf. Proc. 327, Nuclei in the Cosmos III, ed. M. Busso, R. Gallino, & C. M. Raiteri (New York: AIP), 255
de Oliveira, F., et al. 1996, Nucl. Phys. A, 597, 231
———. 1997, Phys. Rev. C, 55, 3149
Descouvemont, P., & Baye, D. 1985, Phys. Rev. C, 31, 2274
Drotleff, H. W., et al. 1993, ApJ, 414, 735
El Eid, M. F., & Champagne, A. E. 1995, ApJ, 451, 298
Endt, P. 1990, Nucl. Phys. A, 521, 1
Endt, P., & van der Leun, C. 1978, Nucl. Phys. A, 310, 1
Forestini, M., & Charbonnel, C. 1997, A&AS, 123, 241
Forestini, M., Goriely, S., Jorissen, A., & Arnould, M. 1992, A&A, 261, 157
Fortune, H. T., & Lacaze, A. G. 2003, Phys. Rev. C, 67, 064305
Fortune, H. T., Powers, J. R., Middleton, R., Bethge, K., & Pilt, A. A. 1978, Phys. Rev. C, 18, 255
Frost, C. A., & Lattanzio, J. C. 1996, ApJ, 473, 383
Funck, C., & Langanke, K. 1989, ApJ, 344, 46
Gallino, R., Arlandini, C., Busso, M., Lugaro, M., Travaglio, C., Straniero, O., Chieffi, A., & Limongi, M. 1998, ApJ, 497, 388
Giesen, U., et al. 1994, Nucl. Phys. A, 567, 146
Gledenov, Yu. M., Salatski, V. I., Sedyshev, P. V., Sedysheva, M. V., Koehler, P. E., Vesna, V. A., & Okunev, I. S. 1995, in AIP Conf. Proc. 327, Nuclei in the Cosmos III, ed. M. Busso, R. Gallino, & C. M. Raiteri (New York: AIP), 173
Goriely, S., & Mowlavi, N. 2000, A&A, 362, 599
Görres, J., Arlandini, C., Giesen, U., Heil, M., Käppeler, F., Leiste, H., Stech, E., & Wiescher, M. 2000, Phys. Rev. C, 62, 5801
Görres, J., Graff, S., Wiescher, M., Azuma, R. E., Barnes, C. A., & Wang, T. R. 1992, Nucl. Phys. A, 548, 414
Graff, S., Görres, J., Wiescher, M., Azuma, R. E., King, J., Vise, J., Hardie, G., & Wang, T. R. 1990, Nucl. Phys. A, 510, 346
Hammache, F., et al. 1998, in Proc. of the Fifth International Symposium on Nuclei in the Cosmos, ed. N. Prantzos & S. Harissopulos (Gif-sur-Yvette: Editions Frontières), 373
Hashimoto, M., Nomoto, K., Arai, K., & Kaminisi, K. 1986, ApJ, 307, 687
Heil, M. 2002, Forschungszentrum Karlsruhe Rep. 6783
Herwig, F. 2000, A&A, 360, 952
Herwig, F., Langer, N., & Lugaro, M. 2003, ApJ, 593, 1056
Hollowell, D., & Iben, I., Jr. 1988, ApJ, 333, L25
Iben, I., Jr., & Renzini, A. 1982, ApJ, 263, L23
Igashira, M., Nagai, Y., Masuda, K., Ohsaki, T., & Kitazawa, H. 1995, ApJ, 441, L89
Iliadis, C., Buchmann, L., Endt, P. M., Herndl, H., & Wiescher, M. 1996, Phys. Rev. C, 53, 475
Iliadis, C., et al. 1990, Nucl. Phys. A, 512, 509
Jorissen, A., & Arnould, M. 1989, A&A, 221, 161
Jorissen, A., & Goriely, S. 2001, Nucl. Phys. A, 688, 508
Jorissen, A., Smith, V. V., & Lambert, D. L. 1992, A&A, 261, 164
Käppeler, F., et al. 1994, ApJ, 437, 396
Karakas, A. I. 2003, Ph.D. thesis, Monash Univ.

Keeley, N., Kemper, K. W., & Khoa, D. T. 2003, Nucl. Phys. A, 726, 159
Kikuchi, T., Nagai, Y., Suzuki, S., Shima, T., Kii, T., Igashira, M., Mengoni, A., & Otsuka, T. 1998, Phys. Rev. C, 57, 2724
King, J. D., Azuma, R. E., Vise, J. B., Görres, J., Rolfs, C., Trautvetter, H. P., & Vlieks, A. E. 1994, Nucl. Phys. A, 567, 354
Koehler, P. E., Kavanagh, R. W., Vogelaar, R. B., Gledenov, Yu. M., & Popov, Yu. P. 1997, Phys. Rev. C, 56, 1138
Kubono, S., et al 2003, Phys. Rev. Lett., 90, 062501
Kuperus, J. 1965, Physica, 31, 1603
Landré, V., Prantzos, N., Aguer, P., Bogaert, G., Lefebvre, A., & Thibaud, J. P. 1990, A&A, 240, 85
Langer, N., Heger, A., Wellstein, S., & Herwig, F. 1999, A&A, 346, L37
Lattanzio, J. C. 1986, ApJ, 311, 708
Lorenz-Wirzba, H., Schmalbrock, P., Trautvetter, H., Wiescher, M., Rolfs, C., & Rodney, W. S. 1979, Nucl. Phys. A, 313, 346
Lugaro, M., Herwig, F., Lattanzio, J. C., Gallino, R., & Straniero, O. 2003, ApJ, 586, 1305
Meissner, J., Schatz, H., Herndl, H., Wiescher, M., Beer, H., & Käppeler, F. 1996, Phys. Rev. C, 53, 459
Mowlavi, N. 1999, A&A, 344, 617
Mowlavi, N., Jorissen, A., & Arnould, M. 1996, A&A, 311, 803
———. 1998, A&A, 334, 153
Nollett, K. M., Busso, M., & Wasserburg, G. J. 2003, ApJ, 582, 1036
Powell, D. C., Iliadis, C., Champagne, A. E., Grossman, C. A., Hale, S. E., Hansper, V. Y., & McLean, L. K. 1999, Nucl. Phys. A, 660, 349
Raman, S., Igashira, M., Dozono, Y., Kitazawa, H., Mizumoto, M., & Lynn, J. E. 1990, Phys. Rev. C, 41, 458
Rauscher, T., Thielemann, F.-K., & Kratz, K.-L. 1997, Phys. Rev. C, 56, 1613
Redder, A., et al. 1982, Z. Phys. A, 305, 325
Renda, A., et al. 2004, MNRAS in press
Schardt, A., Fowler, W. A., & Lauritsen, C. C. 1952, Phys. Rev., 86, 527
Schatz, H., Jaag, S., Linker, G., Steininger, R., Käppeler, F., Koehler, P. E., Graff, S. M., & Wiescher, M. 1995, Phys. Rev. C, 51, 379
Schmidt, S., et al. 1995, Nucl. Phys. A, 591, 227
Seuthe, S., et al. 1990, Nucl. Phys. A, 514, 471
Skelton, R. T., Kavanagh, R. W., & Sargood, D. G. 1987, Phys. Rev. C, 35, 45
Stegmüller, F., Rolfs, C., Schmidt, S., Schulte, W. H., Trautvetter, H. P., & Kavanagh, R. W. 1996, Nucl. Phys. A, 601, 168
Straniero, O., Gallino, R., Busso, M., Chieffi, A., Raiteri, C. M., Salaris, M., & Limongi, M. 1995, ApJ, 440, L85
Thielemann, F.-K., Arnould, M., & Truran, J. W. 1986, in Advances in Nuclear Astrophysics, ed. E. Vangioni-Flam et al. (Gif-sur-Yvette: Editions Frontières), 525
Timmermann, R., Becker, H. W., Rolfs, C., Schröder, U., & Trautvetter, H. P. 1988, Nucl. Phys. A, 477, 105
Travaglio, C., Galli, D., Gallino, R., Busso, M., Ferrini, F., & Straniero, O. 1999, ApJ, 521, 691
Travaglio, C., Gallino, R., Busso, M., & Gratton, R. 2001, ApJ, 549, 346
Utku, S., et al. 1998, Phys. Rev. C, 57, 2731
Utsumi, K. 1985, in Cool Stars with Excesses of Heavy Elements, ed. M. Jaschek & C. Keenan (Dordrecht: Reidel), 243
Vassiliadis, C., & Wood, P. R. 1993, ApJ, 413, 641
Vogelaar, R. B., et al. 1996, Phys. Rev. C, 53, 1945
Wagoner, R. V. 1969, ApJS, 18, 247
Wiescher, M., Görres, J., & Thielemann, F. K. 1990, ApJ, 363, 340
Wiescher, M., & Kettner, K. U. 1982, ApJ, 263, 891
Wilmes, S., Wilmes, V., Staudt, G., Mohr, P., & Hammer, J. W. 2002, Phys. Rev. C, 66, 065802
Wood, P. R., & Zarro, D. M. 1981, ApJ, 247, 247
Zyskind, J. L., & Parker, P. D. 1979, Nucl. Phys. A, 320, 404